DOI: 10.1002/chem.200501005

Biomolecule-Assisted Synthesis and Electrochemical Hydrogen Storage of Porous Spongelike Ni_3S_2 Nanostructures Grown Directly on Nickel Foils

Bin Zhang, Xingchen Ye, Wei Dai, Weiyi Hou, and Yi Xie*[a]

Abstract: Nanothread-based porous spongelike Ni_3S_2 nanostructures were synthesized directly on Ni foil by using a simple biomolecule-assisted method. By varying the experimental parameters, other novel Ni_3S_2 nanostructures could also be fabricated on the nickel substrate. The electrochemical hydrogen-storage behavior of these novel porous Ni_3S_2 nanostructures was investigated as an example of the potential properties of such porous materials. The thread-based porous spongelike Ni_3S_2 could electrochemically charge and discharge with the high capacity of 380 mAh g^{-1} (corresponding to 1.4 wt% hydrogen in single-walled nanotubes (SWNT)). A novel two-charging-plateaux phenomenon was observed in the synthesized porous spongelike Ni_3S_2 nanostructures, suggesting two independent steps in the charging process. We have demonstrated that the morphology of the synthesized Ni_3S_2 nanostructures had a noticeable influence on their electrochemical hydrogen-storage capacity. This is probably due to the size and density of the pores as well as the microcosmic morphology of different nickel sulfide nanostructures. These novel porous Ni_3S_2 nanostructures should find wide applications in hydrogen storage, high-energy batteries, luminescence, and catalytic fields. This facile, environmentally benign, and solution-phase biomolecule-assisted method can be potentially extended to the preparation of other metal sulfide nanostructures on metal substrates, such as Cu, Fe, Sn, and Pb foils.

Keywords: biomolecules · hydrogen storage · nanostructures · nickel · semiconductors

Introduction

During the past few decades, much effort has been focused on designing novel methods to prepare metal chalcogenide nanomaterials. These materials are significant for the understanding of fundamental concepts and offer potential applications in various fields.[1] A variety of methods have been developed for generating metal sulfide nanostructures.[2,3] The biomolecule-assisted synthesis method is a new and promising focus in the preparation of various nanomaterials, because of the special structure of biomolecules.[3] Nanoparticles and one-dimensional nanomaterials of metal sulfides have been prepared with the assistance of macrobiomolecules in the presence of Na_2S or H_2S.[3] However, the pungent H_2S gas was often released during the preparation of sulfides. Therefore, it deserves our special attention to explore a simple, inexpensive, efficient, and environmentally benign biological approach for the high-throughput preparation of metal sulfide nanomaterials. Recently, Komarneni et al. used glutathione (GSH), a large polypeptide molecule, as both the assembling molecule and the sulfur source to synthesize the highly ordered snowflaking structure of bismuth sulfide nanorods under microwave irradiation.[4] In a very recent communication, Qian and co-workers synthesized antimony sulfide nanowires in the presence of cysteine.[5] This inspired us to explore a simpler and more economical method to prepare metal sulfides by using a small biomolecule. Moreover, most of the synthesized metal sulfides were in powder form.[1,2] However, before the possible optical, catalytic, and electrochemical properties of these sulfide nanomaterials, as well as their potential applications, can be identified, their assembly into well-organized nanostructures must be investigated.[6] Recently, the oriented growth of sulfide nanomaterials on substrates was considered as a solution to this difficult problem.[5] Zhang et al. developed a hydrothermal approach to fabricate oriented

[a] Dr. B. Zhang, X. Ye, W. Dai, W. Hou, Prof. Y. Xie
Department of Nanomaterials and Nanochemistry
Hefei National Laboratory for Physical Sciences at Microscale
University of Science and Technology of China
Hefei, Anhui 230026 (P.R. China)
Fax: (+86) 551-360-3987
E-mail: yxie@ustc.edu.cn

Supporting information for this article is available on the WWW under http://www.chemeurj.org/ or from the author.

nanostructured films of metal chalcogenides on metal foils in the presence of powdered sulfur, aqueous hydrazine, and the surfactant cetyltrimethylammonium (CTAB).[7]

Porous materials have attracted attention because of their broad applications in catalysis, biosensors, luminescence, biofiltration, gas storage, magnetics, and heat dissipation.[8–11] For example, nanoporous ZnS nanoparticles demonstrate a very high photocatalytic activity.[9] Suslick et al. also observed that the micro- and macroporous form of MoS_2 had higher thiophene hydrodesulfurization (HDS) activity than that of conventional MoS_2 particles.[10]

Here, we concentrate mainly on the preparation of porous nickel sulfides, because of their good catalytic activity if supported on SiC or $A1_2O_3$.[12] In addition, nickel sulfide is a well-known layered material,[13] and, thus, may exhibit excellent electrochemical properties, as seen from other fullerene-like materials[13–15] (e.g., carbon and MoS_2 nanotubes). Here, we present a novel facile solution-phase biomolecule-assisted method to synthesize Ni_3S_2 nanothread-based porous spongelike structures and other novel nanostructures on a large scale by using hydrothermal treatment of Ni foil and a small biomolecule, L-cysteine ($HSCH_2CH(NH_2)$–COOH). The electrochemical hydrogen-storage behaviors of these novel porous Ni_3S_2 nanostructures were investigated as an example of the potential properties of such porous materials. The nickel sulfide's morphology exerted a marked effect on the electrochemical properties of these nanomaterials.

Results and Discussion

Characterization of structure and morphology of nickel sulfide nanostructures: The X-ray diffraction (XRD) technique was adopted to analyze the crystal structure and phase composition of the products. The powder XRD pattern of the sample is shown in Figure 1, in which the sharp and weak peaks can be indexed to the rhombohedral phase of Ni_3S_2 (JCPDS 85–1802). Moreover, the two strong peaks, attributed to the characteristic peaks of (111) and (200) of Ni foil, can also be observed in this pattern, confirming that Ni_3S_2 nanostructures are developed directly on the Ni substrate. No impurity peaks from other phases were detected, indicating the high purity of the products. X-ray photoelectron spectroscopy (XPS) was also used to analyze the atomic ratio of Ni to S in the samples obtained. The two strong peaks at around 856.4 and 874.2 eV displayed in Figure 2a

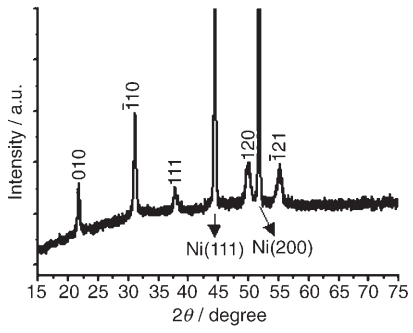

Figure 1. XRD pattern of the spongelike nickel sulfide prepared from 0.769 g Ni foil, 2 mmol L-cysteine, and 20 mL H_2O at 120 °C for 24 h. This pattern indicates that the product is the rhombohedral phase of Ni_3S_2 with high crystallinity.

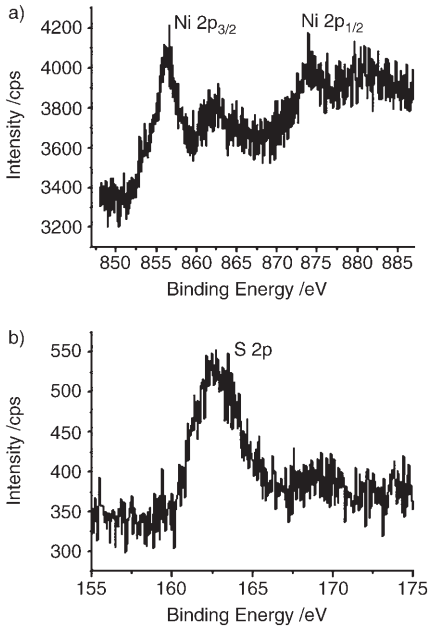

Figure 2. XPS spectra of the nanothread-based porous spongelike Ni_3S_2 nanostructures prepared from 0.769 g Ni foil, 2 mmol L-cysteine, and 20 mL H_2O at 120 °C for 24 h. a) Ni 2p; b) S 2p.

can be attributed to Ni $2p_{3/2}$ and Ni $2p_{1/2}$, respectively. The peak at 162.5 eV in Figure 2b can be assigned to S 2p. Taking into account the atomic sensitivity factor of S and Ni, the atomic ratio of Ni:S is approximately 3:2, revealing the stoichiometric composition of Ni_3S_2. No peaks of elements other than Ni, S, C, and O are observed in the wide XPS spectrum (Figure S1, Supporting Information), which further confirms the high purity of the Ni_3S_2 product.

The morphology of the Ni_3S_2 products prepared was also examined by using field emission scanning electron microscopy (FESEM). Figure 3 shows low-magnification SEM images of porous nickel sulfide nanostructures on Ni foils following the hydrothermal treatment of 0.769 g of nickel foil and 2 mmol cysteine in distilled water at 120 °C. The low-magnification FESEM image (Figure 3a) shows the products to be irregular porous spheres with morphologies very similar to the MoS_2 netlike nanostructures prepared by using the ultrasonic spray pyrolysis (USP) method with a sacrificial colloidal silica template.[10] These latter products were in powder form and were obtained at 700 °C by using USP apparatus, whereas our biomolecule-assisted approach requires a very low temperature and the porous samples are grown directly on nickel foil substrate. A high-magnification

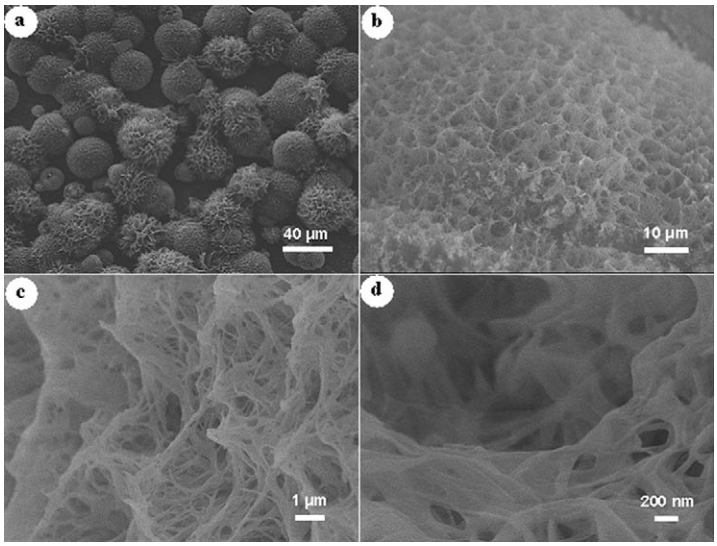

Figure 3. Typical SEM images of porous nickel sulfide nanostructures grown on Ni foils at different magnifications. The products were prepared from 0.769 g of nickel foil and 2 mmol cysteine hydrothermally treated in Milli-Q water at 120 °C.

SEM image (Figure 3b) further shows that the nickel sulfide samples prepared are porous structures. The microstructure of the porous Ni_3S_2 can be seen even more clearly in the higher-magnification SEM image shown in Figure 3c. This demonstrates that the porous spongelike nickel sulfide nanostructure is composed of nanothreads with a diameter of 60–400 nm. The image in Figure 3d shows that the nanothreads in the porous products are quite flexible. These SEM results reveal that the porous spongelike nickel sulfide nanostructures can be developed directly on the Ni substrate on a large scale.

Influence of reaction temperature and mass of cysteine: The reaction temperature and the mass of cysteine are vital factors in the synthesis and control of the morphology of the Ni_3S_2 nanostructures grown directly on Ni foils. As the hydrothermal temperature was decreased to 90 °C, compact and uniform films were obtained directly on the substrate (Figure 4a). A high-magnification SEM image (Figure 4b) shows that the Ni_3S_2 film obtained is composed of vertically aligned nanoflake arrays. As the mixture of 0.769 g Ni foil, 3 mmol L-cysteine, and 20 mL H_2O was maintained under hydrothermal conditions at 90 °C for 24 h, flakelike porous Ni_3S_2 nanostructures were observed (Figure 4c). In contrast to the samples shown in Figure 3, this product was composed of flakes, and the arrangement of flakes was more compact and the pores were smaller. By decreasing the mass of cysteine to 2 mmol and increasing the hydrothermal temperature 150 °C, compactly arranged Ni_3S_2 spheres could be developed directly on the nickel foil. As seen in Figure 4d, the products are composed of Ni_3S_2 microspheres deposited on the Ni substrate, with an average diameter of 900 nm. Note that the structure and phase composition of all three samples obtained under different conditions proved to be the pure rhombohedral phase of Ni_3S_2 established from XRD analysis. Hence, the successful preparation of novel porous Ni_3S_2 nanostructures reveals that L-cysteine does not only function as a sulfur source, but also as the shape-controlling agent in the synthesis of Ni_3S_2 nanostructures on nickel foils. This indicates that the morphologies of the porous nickel nanostructures are sensitive to the hydrothermal temperature.

The mechanism of formation of the porous Ni_3S_2 nanostructures: If the reaction solutions were initially deaerated with N_2 for 15 min without changing the other experimental conditions, the nickel sulfide nanostructures could not be obtained on the Ni foil surface. This suggests that O_2 is required for the formation of the nanostructures. Nickel ions may be released during the reaction between the nickel foil and O_2, which is consistent with the observations of Wen et al. of the growth of $Cu(OH)_2$ nanostructures on Cu foils.[15] In the cysteine molecule, there are many functional groups, such as $-NH_2$, $-COOH$, and $-SH$, that have a strong tendency to coordinate with inorganic cations and metals. Based on observations from mass spectrometry, Burford and co-workers reported that metal ions could react with cysteine to form complexes.[16] Therefore, it is reasonable to conclude that, in our approach, the released Ni^{2+} on the nickel foil can coordinate with cysteine to form initial precursor complexes. In the following process, the coordination bonds between the hydrosulfide group and Ni^{2+} rupture because of the high reaction temperature (120 °C). The proposed reaction procedure is shown in Scheme 1.

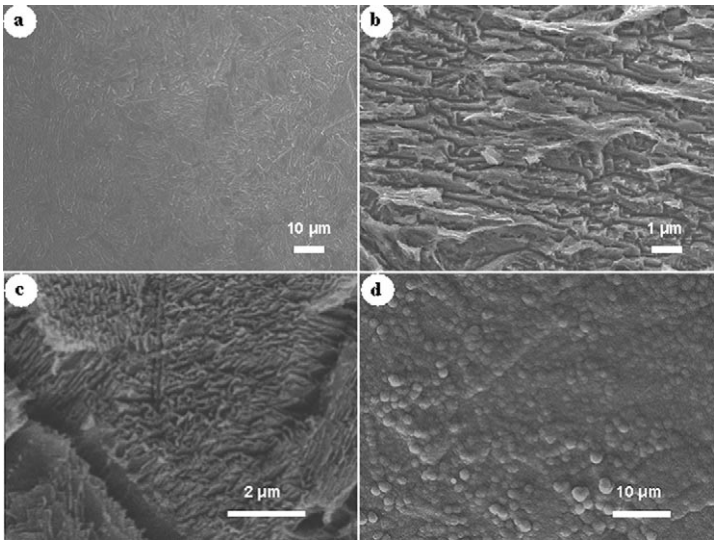

Figure 4. SEM images of Ni_3S_2 nanostructures grown directly on nickel foils by adopting the biomolecule-assisted method under different experimental conditions. a,b) Flake-based Ni_3S_2 films obtained from 0.769 g Ni foil, 2 mmol L-cysteine, and 20 mL H_2O at 90 °C for 24 h. c) Flakelike porous Ni_3S_2 nanostructures prepared from 0.769 g Ni foil, 3 mmol L-cysteine, and 20 mL H_2O at 90 °C for 24 h. d) Compactly arranged Ni_3S_2 spheres obtained from 0.769 g Ni foil, 2 mmol L-cysteine, and 20 mL H_2O at 150 °C for 24 h.

$$Ni + O_2 + H_2O \xrightarrow{\Delta} Ni^{2+} + OH^-$$

$$Ni^{2+} + n(\text{L-cysteine}) \xrightarrow{\text{coordination}} [Ni(\text{L-cysteine})_n]^{2+}$$

$$[Ni(\text{L-cysteine})_n]^{2+} \xrightarrow[\Delta]{\text{Ni-S rupture}} Ni_3S_2$$

Scheme 1. A possible mechanism for the formation of nickel sulfide nanostructures on Ni foils.

To form further nanostructures of nickel sulfide on the surface of Ni foil, the Ni ions must be constantly transferred to the initially grown Ni_3S_2 surface. Therefore, channels for the transfer of nickel ions on the Ni_3S_2 surfaces must exist. As the sulfur source of L-cysteine was completely consumed, these channels remained and became pores in the final products (see Figures 3 and 4a–c). To investigate the effect of the Ni substrate on the growth of nickel sulfide nanomaterials, we replaced the Ni foil with Ni and $NiCl_2$ powders, respectively. Interestingly, only spherical samples of nickel sulfide were obtained. The XRD measurements demonstrate that the former product is the rhombohedral phase of Ni_3S_2 (not shown), whereas the latter samples, obtained by using $NiCl_2$ as the nickel source, are the cubic phase of NiS_2 (see Figure S2, Supporting Information). This suggests that the nickel ions are released omnidirectionally from the Ni powder and $NiC1_2$,[7] and reveals that the Ni source plays an important role in the morphology and structure of nickel sulfide nanomaterials. This further confirms that the release rate of Ni^{2+} is essential for the growth of novel porous nanostructures in our biomolecule-assisted method. The presence of L-cysteine molecules, which have a strong tendency to coordinate with nickel ions, can decrease the rate of formation of Ni^{2+} and cause the Ni^{2+} to be released slowly from the surface of Ni foil. If the temperature is kept relatively low (90 °C), nickel ions can be released uniformly from the Ni foil, and, thus, nickel sulfide nanostructures can be developed uniformly from the substrate to form Ni_3S_2 film (Figure 4a,b). We are conducting further systematic work to improve the understanding of the formation mechanism of porous spongelike Ni_3S_2 nanostructures.

The hydrogen storage of the porous Ni_3S_2 nanostructures obtained: The porous nickel sulfide nanostructures prepared were shown to have excellent electrochemical hydrogen-storage capacity. Figure 5 displays the charge/discharge voltage difference of porous spongelike nickel sulfide nanostructures as a function of capacity at a constant current density of 30 mA g^{-1}. The charge curve (Figure 5a) reveals a voltage plateau from 0 to 120 mAh g^{-1}. As the electrochemical capacity increases, the potential decreases quickly to −1.5 V and remains unchanged as the charge capacity reaches 158 mAh g^{-1}. A second voltage potential plateau is observed between 158 and 360 mAh g^{-1}. This indicates that two different hydrogen-adsorption sites exist in the porous spongelike Ni_3S_2 nanostructures; in other words, there are two different electrochemical steps in the charging process. It was assumed that the hydrogen initially adsorbed into the pores of nickel sulfide and then entered the interstitial sites between layers (the layered structure of nickel sulfide). This two-plateaux phenomenon was also observed in the flake-based porous Ni_3S_2 nanostructures electrode (Figure 5c). However, in compactly arranged Ni_3S_2 spheres, only one charging plateau is seen (Figure 5d), providing proof for the above-mentioned assumption. In fact, a similar two-step hydrogen-adsorption mechanism of single-walled carbon nanotubes was proposed by Lee et al. on the basis of density functional calculations.[17] As shown in Figure 5a, the plateau of the discharging potential is observed at approximately −1.4 V and the discharging capacity of 380 mAh g^{-1} can be obtained, which amounts to a hydrogen-storage capacity of 1.4 wt % in SWNTs.[18] The value of the discharging capacity is higher than those of MoS_2, boron nitride (BN) nanotubes as well as selenium submicrotubes.[18b,19,20] This indicates that this type of nickel sulfide nanostructure can be applied as the materi-

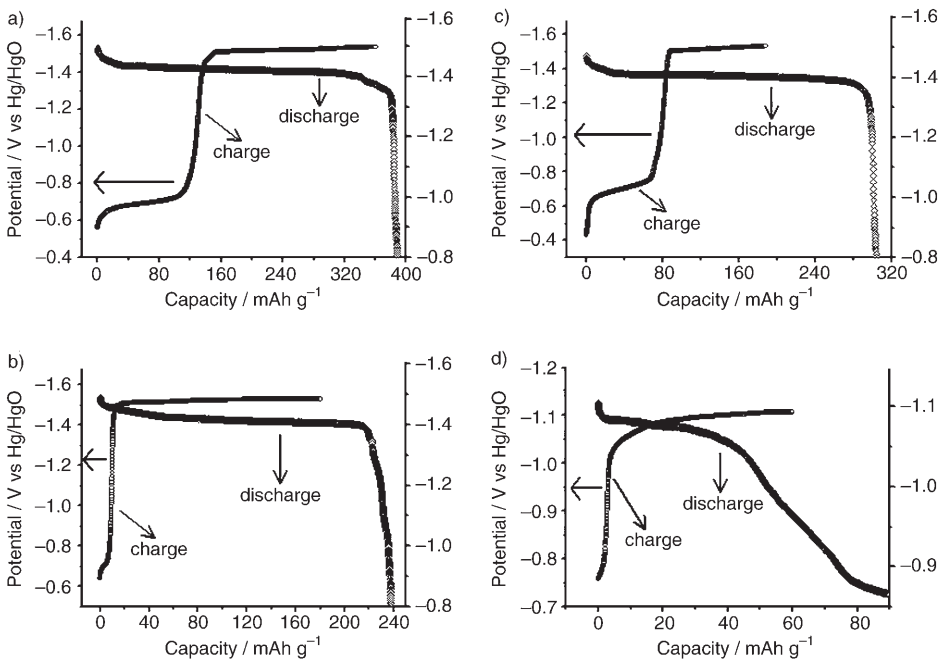

Figure 5. Charge/discharge curves of the different Ni_3S_2 nanostructures electrodes at a constant current density of 30 mA g^{-1}. a) Nanothread-based porous spongelike nanostructures; b) flake-based Ni_3S_2 films; c) flakelike porous Ni_3S_2 nanostructures; d) compactly arranged Ni_3S_2 spheres. The thick lines show the axis of the charging curve.

al of electrochemical hydrogen storage. The high capacity was considered to be pertinent to the enhanced electrocatalytic activity of the highly porous and layered structures of the synthesized Ni_3S_2. The discharge capacity of the material decreases by only 0.5% after a preliminary test of ten consecutive charge/discharge cycles, suggesting the good reversibility of hydrogen storage. Replacement of the electrode material by the vertically aligned nanoflakes-based film of Ni_3S_2 resulted in the decrease in the discharge capacity to 218 mAh g^{-1} (0.78 wt% hydrogen in SWNTs, Figure 5b), which reveals that the capacity of electrochemical hydrogen storage of the final products is sensitive to the morphology of nickel sulfide. Although there are two voltage plateaux in the charge curve of the vertically aligned nanoflakes film electrode, the first potential plateau is very weak and almost imperceptible (Figure 5b). Careful analysis of its SEM images revealed that there are a few spaces/pores in the vertically aligned nanoflakes films (Figure 4b). Therefore, the pores are undoubtedly responsible for the first charging potential plateau and play an important role in hydrogen-storage capacity. For the flakelike porous Ni_3S_2 nanostructures electrode, the value of discharge capacity is 293 mAh g^{-1}, whereas the discharge capacity of compactly arranged Ni_3S_2 spheres is only 70 mAh g^{-1}, lower than that of porous spongelike Ni_3S_2 nanostrucutres. This further confirms that the morphologies exert a noticeable influence on the electrochemical hydrogen-storage ability of Ni_3S_2 on nickel foils, and also indicates that the porous structure of the nickel sulfide products is a crucial factor for the high hydrogen-storage ability of Ni_3S_2 nanostrucutres. To demonstrate the influence of the morphology on the hydrogen-storage capacity of Ni_3S_2 nanostructures on nickel foils, the morphologies and their corresponding discharging capacities are displayed in Table S1 in the Supporting Information. A simple charge/discharge mechanism of Ni_3S_2 nanostructures is proposed in Scheme 2. It is concluded that the size and density of pores as well as the microcosmic morphology of different nickel sulfide nanostructures resulted in differences in the electrochemical capacity of hydrogen storage.

$$Ni/Ni_3S_2 + H_2O + e^- \underset{\text{discharge}}{\overset{\text{charge}}{\rightleftharpoons}} Ni/H_{ad}/Ni_3S_2 + OH^-$$

Scheme 2. A proposed mechanism for the electrochemical hydrogen storage of Ni_3S_2 nanostructures.

Conclusion

In summary, a novel simple L-cysteine-assisted hydrothermal method has been developed to synthesize nanothread-based porous spongelike nanostructures on Ni foil in a high yield at a low temperature. By varying the experimental parameters, other morphologies of Ni_3S_2 nanostructures (including nanoflake-based film of Ni_3S_2 and flakelike porous Ni_3S_2 nanostructures and compactly arranged Ni_3S_2 spheres) could also be obtained. We have demonstrated that these novel nickel sulfide nanomaterials grown on Ni foils could electrochemically charge and discharge with a maximum capacity of 380 mAh g^{-1} (corresponding to 1.4 wt% hydrogen in SWNTs). The capacity of electrochemical hydrogen storage was susceptible to the morphology and structure of nickel sulfide nanostructures. These novel porous Ni_3S_2 nanostructures should find applications in the fields of hydrogen storage, high-energy batteries, luminescence, and catalysis. In addition, this facile, environmentally benign, and solution-phase biomolecule-assisted method can be potentially extended to the preparation of other metal sulfide nanostructures on metal substrates, such as Cu, Fe, Sn, Pb foils.

Experimental Section

Synthesis of the porous Ni_3S_2 nanostructures: In a typical procedure, nickel foil was rinsed with acetone followed by ethanol twice. L-Cysteine (2 mmol), fresh Milli-Q water (20 mL), and nickel foil (0.769 g, purity: 99.99%, thickness: 0.2 mm) were placed into a 50 mL Teflon-lined autoclave. The autoclave was sealed, maintained at 120°C for 24 h, and then allowed to cool to room temperature. The Ni foil was collected and washed with absolute ethanol followed by water three times. The sample was then dried in vacuum at 50°C for 6 h.

Characterization: The X-ray diffraction (XRD) patterns of the products were recorded by using a Rigaku Dmax Diffraction System with a $Cu_{K\alpha}$ source ($\lambda = 0.154178$ nm). The scanning electron microscopy images were taken by using a JEOL-JSM-6700F field-emitting scanning electron microscope (FESEM, 15 kV). Transmission electron microscopy (TEM) images and electron diffraction patterns were obtained with a Hitachi 800 system at 200 kV. The specimens for TEM measurements were prepared by spreading a droplet of ethanol suspension onto a copper grid that was coated with a thin layer of amorphous carbon film, and allowed to air dry. X-ray photoelectron spectroscopy (XPS) was performed by using an ESCALAB MK II X-ray photoelectron spectrometer with non-monochromatized $Al/Mg_{K\alpha}$ X-ray as the excitation source.

Electrochemical hydrogen storage: The electrochemical measurements were taken by following the method reported in ref. [14a] with slight modification. Briefly, the electrode was fabricated by welding directly the nickel foil with the Ni_3S_2 nanostructures on a sheet of nickel foam. The active Ni_3S_2 samples were estimated by using the sulfur content of L-cysteine on the assumption that the sulfur component of cysteine was completely transformed into Ni_3S_2. The calculation method is reasonable and conservative because in our electrochemical measurements the only sulfur source of the final products is L-cysteine ($HSCH_2CH(NH_2)COOH$). All the experiments were performed in a three-electrode cell in 5 M KOH at 25°C under normal atmosphere. The Ni_3S_2 nanostructures (including the nickel foil) were used as the working electrode, $Ni(OH)_2/NiOOH$ as the counter electrode, and Hg/HgO as a reference electrode. The Ni_3S_2 nanostructures electrode was charged for 3 h at a current density after a 2 s rest. All the electrochemical hydrogen-storage experiments were carried out by using the Land battery system (CT2001A).

Acknowledgements

This work was supported by the National Nature Science Foundation (NSF) of China.

[1] a) J. Hu, T. W. Odom, C. M. Liber, *Acc. Chem. Res.* **1999**, *32*, 435; b) G. M. Whitesides, B. Grzybowski, *Science* 2002, 295, 2418; c) M. A. El-Sayed, *Acc. Chem. Res.* **2004**, *37*, 326; d) Y. L. Wang, L. Xia, Y. N. Xia, *Adv. Mater.* **2005**, *17*, 473.

[2] a) M. B. Sigman, Jr., B. A. Korgel, *Chem. Mater.* **2005**, *17*, 1655; b) W. P. Lim, Z. H. Zhang, H. Y. Low, W. S. Chin, *Angew. Chem.* **2004**, *116*, 5803; *Angew. Chem. Int. Ed.* **2004**, *43*, 5685; c) C. H. Ye, G. W. Meng, Z. Jiang, Y. H. Wang, G. Z. Wang, L. D. Zhang, *J. Am. Chem. Soc.* **2002**, *124*, 15180; d) Y. D. Li, X. L. Li, R. R. He, J. Zhu, Z. X. Deng, *J. Am. Chem. Soc.* **2002**, *124*, 1411.
[3] C. B. Mao, D. J. Solis, B. D. Reiss, S. T. Kottmann, R. Y. Sweeney, A. Hayhurst, G. Georgiou, B. Iverson, A. M. Belcher, *Science* **2004**, *303*, 213, and references therein.
[4] Q. Lu, F. Gao, S. Komarnei, *J. Am. Chem. Soc.* **2004**, *126*, 54.
[5] X. Y. Chen, X. F. Zhang, C. W. Shi, X. L. Li, Y. T. Qian, *Solid State Commun.* **2005**, *134*, 613.
[6] Y. F. Chan, X. F. Duan, S. K. Chan, I. K. Sou, X. X. Zhang, N. Wang, *Appl. Phys. Lett.* **2003**, *83*, 2665.
[7] L. Z. Zhang, J. C. Yu, M. S. Mo, L. Wu, Q. Li, K. W. Kwong, *J. Am. Chem. Soc.* **2004**, *126*, 8116, and references therein.
[8] a) M. R. Buchmeiser, *Angew. Chem.* **2001**, *113*, 3911; *Angew. Chem. Int. Ed.* **2001**, *40*, 3795; b) Y. Shin, J. Liu, L. Q. Wang, Z. Nie, W. D. Samuels, G. E. Fryxell, G. J. Exarhos, *Angew. Chem.* **2000**, *112*, 2814; *Angew. Chem. Int. Ed.* **2000**, *39*, 2702; c) L. Z. Zhang, J. C. Yu, Z. Zheng, C. W. Leung, *Chem. Commun.* **2005**, 2683; d) H. W. Gu, R. K. Zheng, H. Liu, X. X. Zhang, B. Xu, *Small* **2005**, *1*, 402; e) P. Sozzani, S. Bracco, A. Comotti, L. Ferretti, R. Simonutti, *Angew. Chem.* **2005**, *117*, 1850; *Angew. Chem. Int. Ed.* **2005**, *44*, 1816; f) C. Barner-Kowollik, H. Dalton, T. P. Davis, M. H. Stenzel, *Angew. Chem.* **2003**, *115*, 3792; *Angew. Chem. Int. Ed.* **2003**, *42*, 3664.
[9] J. S. Hu, L. L. Ren, Y. G. Guo, H. P. Liang, A. M. Cao, L. J. Wan, C. L. Bai, *Angew. Chem.* **2005**, *117*, 1295; *Angew. Chem. Int. Ed.* **2005**, *44*, 1269.
[10] a) S. E. Skrabalak, K. S. Suslick, *J. Am. Chem. Soc.* **2005**, *127*, 9990; b) W. H. Suh, K. S. Suslick, *J. Am. Chem. Soc.* **2005**, *127*, 12007.
[11] a) A. Müller, D. Rehder, E. T. K. Haupt, A. Merca, H. Bögge, M. Schmidtmann, G. Heinze-Brückner, *Angew. Chem.* **2004**, *116*, 4566; *Angew. Chem. Int. Ed.* **2004**, *43*, 4466; b) L. Jiang, Y. Zhao, J. Zhai, *Angew. Chem.* **2004**, *116*, 4438; *Angew. Chem. Int. Ed.* **2004**, *43*, 4338; c) C. Serre, F. Millange, S. Surblé, G. Férey, *Angew. Chem.* **2004**, *116*, 6445; *Angew. Chem. Int. Ed.* **2004**, *43*, 6285; d) C. Liang, K. Hong, G. A. Guiochon, J. W. Mays, S. Dai, *Angew. Chem.* **2004**, *116*, 5909; *Angew. Chem. Int. Ed.* **2004**, *43*, 5785; e) S. Kitagawa, R. Kitaura, S. Noro, *Angew. Chem.* **2004**, *116*, 2388; *Angew. Chem. Int. Ed.* **2004**, *43*, 2334.
[12] a) J. M. Ledoux, C. Pham-Huu, N. Keller, J. B. Nougayrède, S. Savin-Poncet, J. Bousquet, *Catal. Today* **2000**, *61*, 157; b) S. C. Paik, J. S. Chung, *Appl. Catal. B* **1996**, *8*, 267.
[13] a) R. Tenne, *Angew. Chem.* **2003**, *115*, 5280; *Angew. Chem. Int. Ed.* **2003**, *42*, 5124; b) M. Remškar, *Adv. Mater.* **2004**, *16*, 1497.
[14] a) G. P. Dai, C. Liu, M. Liu, M. Z. Wang, H. M. Cheng, *Nano Lett.* **2002**, *2*, 503; b) A. M. Seayad, D. M. Antonelli, *Adv. Mater.* **2004**, *16*, 765; c) G. Gundiah, A. Govindaraj, N. Rajalakshmi, K. S. Dhathathreyan, C. N. R. Rao, *J. Mater. Chem.* **2003**, *13*, 209.
[15] X. G. Wen, W. X. Zhang, S. H. Yang, *Langmuir* **2003**, *19*, 5898.
[16] N. Burford, M. D. Eelman, D. E. Mahony, M. Morash, *Chem. Commun.* **2003**, 146.
[17] S. M. Lee, K. H. An, Y. H. Lee, G. Seifert, T. Frauenheim, *J. Am. Chem. Soc.* **2001**, *123*, 5059.
[18] a) N. Rajalakshmi, K. S. Dhathathreyan, A. Govindaraj, B. C. Satishkumar, *Electrochim. Acta* **2000**, *45*, 4511; b) J. Chen, N. Kuriyama, H. Yuan, H. T. Takeshita, T. Sakai, *J. Am. Chem. Soc.* **2001**, *123*, 11813; c) C. Nützenadel, A. Züttel, D. Chartouni, L. Schlapbach, *Electrochem. Solid-State Lett.* **1999**, *2*, 30.
[19] X. Chen, X. P. Gao, H. Zhang, Z. Zhou, W. K. Hu, G. L. Pan, H. Y. Zhu, T. Y. Yan, D. Y. Song, *J. Phys. Chem. B* **2005**, *109*, 11525.
[20] B. Zhang, W. Dai, X. Ye, W. Hou, Y. Xie, *J. Phys. Chem. B* **2005**, *109*, 22830.

Received: August 17, 2005
Published online: January 3, 2006

